





Surface prereacted glass-ionomer particles incorporated into resin composites promote biocompatibility for restoration of subgingival dental defects

Yueyi Yang^{a,b,c,1}, Jing Huang^{a,b,c,1} , Xuchen Hu^{a,b,c},
Meiling Jing^{a,b,c}, Yujie Zhang^{a,b,c}, Chenci Xu^d, Wenduo Tan^{a,b,c}, Xiaoyu Liu^{a,b,c},
Chenguang Niu^{a,b,c,**}, Zhengwei Huang^{a,b,c,*} 

^a Department of Endodontics, Shanghai Ninth People's Hospital, Shanghai Jiao Tong University School of Medicine, College of Stomatology, Shanghai Jiao Tong University, Shanghai, China

^b National Clinical Research Center for Oral Diseases, National Center for Stomatology, Shanghai, 200011, China

^c Shanghai Key Laboratory of Stomatology, Shanghai, 200011, China

^d Department of Oral and Cranio-maxillofacial Surgery, Shanghai Ninth People's Hospital, Shanghai Jiao Tong University School of Medicine, China

ARTICLE INFO

Keywords:

Surface prereacted glass ionomer
Cytocompatibility
Osteogenesis
Angiogenesis
Subgingival dental defect

ABSTRACT

Subgingival dental defects are common in clinical practice among patients with deep dental caries and dental fractures. These defects commonly accompany lesions involving marginal alveolar bone loss and gingival recession, and their clinical management is challenging. Restoring gingival adhesion and activating the regeneration of periodontal tissue are important for a better prognosis in these cases. However, there is no effective resin material for complex restorations involving the destruction of subgingival tissue. To achieve greater biocompatibility, resins are generally modified with bioactive particles that can release specific components. Surface prereacted glass ionomer (S-PRG) is a novel glass particle characterized by a three-layered structure and the release of multiple ions with bioactive potential. Therefore, in this study, we incorporated S-PRG filler into resin-based composites to investigate their effectiveness in the restoration of subgingival defects. Resin composites containing 0, 10, 30, 50, or 70 wt% S-PRG filler were fabricated and formed into material discs, where a commercial resin composite served as the control group. The microstructure and elemental distribution were characterized by scanning electronic microscopy and energy-dispersive spectroscopy. The resin composites containing 50 or 70 wt% S-PRG fillers exhibited comprehensively better physicochemical properties, including flexural modulus, compressive strength, and water sorption. The ion release profile and environmental pH of the resins were measured with material extracts. Periodontal ligament stem cells were considered as seed cells that harbored great potential for periodontal regeneration. Cellular experiments suggested that S-PRG promotes cell proliferation and adhesion, induces cell migration, and stimulates vascularized osteogenesis. The feasibility of using S-PRG-containing resin composite to rectify subgingival dental defects was confirmed *in vivo*. After restoration with the S-PRG-filled resin material, intact epithelial tissue adhered to the resin surface with no visible inflammation. In conclusion, S-PRG-filled resin composites showed some biocompatibility as an alternative material for clinical applications.

1. Introduction

Subgingival dental defects are common in clinical practice, and their treatment is often complex [1]. The margin of defects that extend below

the cemento–enamel junction predominantly occurs in deep dental caries and dental fractures [2]. The restoration of subgingival cavities of such dimensions poses a clinical challenge. In addition to surgical problems, such as tooth preparation and contamination control, the

* Corresponding author. No. 639 Zhizaoju Road, Shanghai, 200011, China.

** Corresponding author. No. 639 Zhizaoju Road, Shanghai, 200011, China.

E-mail addresses: niuchg09@alumni.sjtu.edu.cn (C. Niu), huangzhengwei@shsmu.edu.cn (Z. Huang).

¹ These authors contributed equally to this study.

prevention of further lesions in neighboring soft and hard tissues is difficult to achieve. Restoring gingival adhesion and maintaining its biological width are important in ensuring a good prognosis [3,4]. More importantly, subgingival defects are often accompanied by marginal bone loss and gingival recession under certain circumstance, especially when deep caries in the distal surface are associated with impacted wisdom teeth [5,6]. There are three alternative clinical procedures for the restoration of subgingival lesions. Whereas surgical crown lengthening and orthodontic forced eruption pose a risk of injury to the surrounding tissue, the technique of deep margin elevation utilizes a composite resin in the proximal area to relocate the cervical margin supragingivally in a noninvasive way [7–9]. Therefore, to resolve the clinical problems associated with subgingival dental defects accompanied by tissue lesions, resin composites with some degree biocompatibility must be investigated.

In recent years, various bioactive materials have been studied for use in dentistry, with most attention focused on osteogenic formation and remineralization [10]. However, the capacity of these materials to restore gingival adhesion and promote the regeneration of hard and soft tissues must also be considered [11,12]. To achieve various biofunctions, particles that release specific components are used to modify dental materials [13]. Surface prereacted glass ionomer (S-PRG) filler, which was originally developed by Shofu Inc. (Kyoto, Japan), is a glass powder generated from multifunctional glass (fluoroboroaluminosilicate glass) as the raw material. This bioactive material is characterized by a three-layer structure with a prereacted glass-ionomer phase on the surface of the glass filler core, which stably releases multiple ions. The structure and ion-storage-battery-like function allows the S-PRG filler to interact with living tissue and to affect the biological environment [14–16]. A series of bioactive functions displayed by S-PRG filler has been reported, involving increased cell viability [17, 18], acid neutralization [19], antibacterial effects [20,21], and the promotion of mineralization [22]. In the experiments cited above, the S-PRG filler was incorporated into cements, root canal sealers, and computer aided design/computer-aided manufacturing composites, among others, to demonstrate its different therapeutic effects. However,

the effect of S-PRG filler in restoring gingival adhesion sites and activating periodontal regeneration have not been investigated, although they are important in restoration and prognosis of subgingival defects.

The purpose of regenerating the periodontal tissue in subgingival defects is to reverse the marginal alveolar bone loss, restore the adhesion of soft tissue, and maintain the biological width. The discovery of stem cells with enormous proliferative activity and multipotency offers new hope for the regeneration of functional tissues [23]. Periodontal ligament stem cells (PDLSCs) are a subgroup of dental stem cells that can be isolated from the periodontal ligament. These cells can differentiate into multiple cell lineages and may be involved in the healing of periodontal lesions [24–26]. In this study, we incorporated S-PRG filler into resin-based composites, as illustrated in Fig. 1. Resin composites containing 0, 10, 30, 50, or 70 wt% S-PRG filler were generated and formed into material discs with 15 mm diameters and 1 mm thickness. The morphology and hydrophilicity of the material surfaces were determined to establish the content of S-PRG filler suitable for optimizing cell adhesion and proliferation. The material discs were then shown to release bioactive ions and alter the pH of the environment. *In vitro* experiments were performed to investigate the effects of the modified resins on the cytocompatibility of the material, osteogenic differentiation, and vascular development. The migration of human PDLSCs (hPDLSCs) was visualized to assess the potential of S-PRG filler to interfere with soft tissue and to induce adhesion. The feasibility of using these resins to resolve subgingival dental defects was examined *in vivo* using a commercial flowable resin composite containing S-PRG filler. The results of this study demonstrate that S-PRG induces gingival adhesion and shows a degree of biocompatibility, which allow the regeneration of periodontal tissue.

2. Materials and methods

2.1. Fabrication of S-PRG-filled resin composite discs

The S-PRG-filled resin composite discs were provided by Shofu Inc., Japan. The manufacturing process was illustrated in Fig. S1 A, which

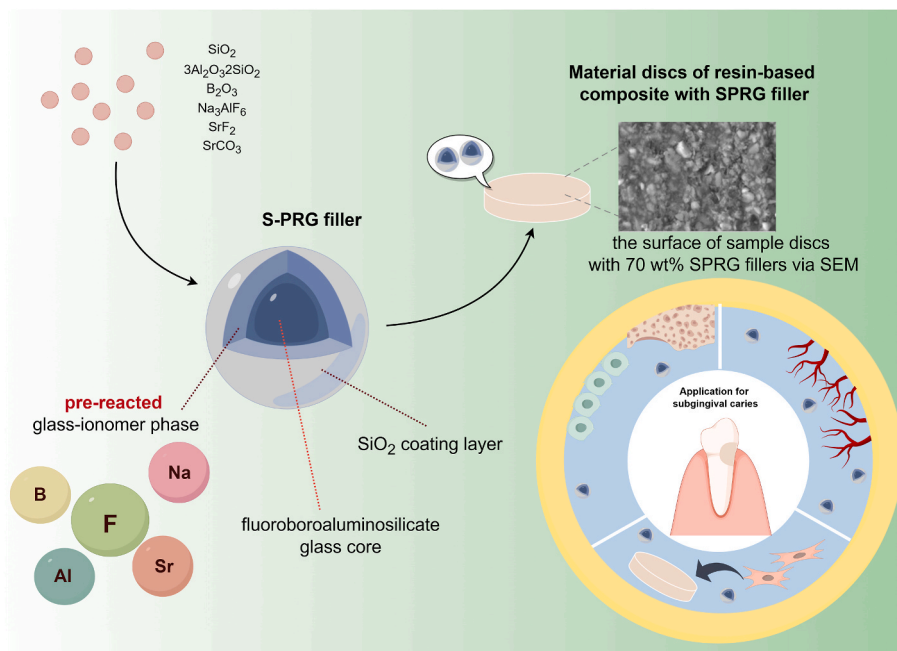


Fig. 1. Scheme of S-PRG-filling resin composites for subgingival dental defects restorations. S-PRG filler is a glass particle composed of three layers: outer SiO_2 coating layer; prereacted glass-ionomer phase; fluoroboroaluminosilicate glass core in the innermost layer. S-PRG filler functions as an ion-storage battery, releasing multiple ions: fluoride, borate, strontium, sodium, and aluminum. S-PRG filler was incorporated into resin-based composites, which were fashioned into material discs. These were used in subsequent experiments to investigate the effects of S-PRG on cell adhesion, vascularized bone regeneration, and the restoration of subgingival dental defects.

was created in <https://BioRender.com>. Briefly, the ingredients of S-PRG, including 14.0 wt% silica (SiO₂), 27.0 wt% mullite (3Al₂O₃·2SiO₂), 19.0 wt% boric oxide (B₂O₃), 5.0 wt% cryolite (Na₃AlF₆), 29.0 wt% strontium fluoride (SrF₂), and 6.0 wt% of strontium carbonate (SrCO₃), were mixed and melted at 1400 °C in an arc furnace for 2 h. The liquid mixture was quenched in running water and dried for 12 h at 150 °C in an air oven to obtain fluoroboroaluminosilicate glass frit. The glass frit was coarsely ground for 12 h with a ball mill (BM-10, Seiwa Giken Co., Hiroshima, Japan), and wet ground with an agitator bead mill to a mean particle size of about 1.0 μm (measured with a laser diffraction particle size measuring instrument; Nikkiso Co., Ltd, Tokyo, Japan). Polysiloxane solution (16 wt% SiO₂; 2–6 degrees of condensation; Mitsubishi Chemical Co., Tokyo, Japan) was added to the glass slurry, which was then agitated. After aging for 40 h at 50 °C and heat treatment for 6 h at 120 °C in a heat dryer, the solidified material was disintegrated in a cutter mixer and subjected to a spray treatment with polyacrylic acid aqueous solution (13.0 wt% polymer content) to obtain the surface-treated glass filler. The S-PRG filler was obtained after heating in a heat dryer for 3 h at 150 °C.

To create the resin composites containing S-PRG fillers, a resin matrix was obtained by mixing monomers (Bis-GMA/TEGDMA, 69.7/29.7, wt/wt) and a photoinitiator system (CQ/EDMAB, 0.3/0.3, wt/wt). Then, S-PRG fillers with different mass fractions were blended with the resin matrix. The mass fractions of different groups were shown in Table 1. The samples were filled into a metal mold of 15 mm diameter and 1 mm thickness, pressed from both sides with cover glass, and light-cured at four different positions for 3 min each side with a halogen lamp (Shofu Inc., Japan; wavelength 400–550 nm, 600 W, Solidilite V).

The experimental resin composites were denoted as G0 (S-PRG filling: 0 wt%), G10 (S-PRG filling: 10 wt%), G30 (S-PRG filling: 30 wt%), G50 (S-PRG filling: 50 wt%), and G70 (S-PRG filling: 70 wt%), respectively. G0 samples were used as a control. Meanwhile, the commercial dental resin composites (Minnesota Mining and Manufacturing Corporation, USA), denoted as FZ, were selected as a positive control for the following experiments. The optical images of disc-shaped S-PRG-filling resin composites and FZ were shown in Fig. S1 B.

2.2. Preparation of material extraction medium

The material extraction medium was prepared under sterile conditions, using complete medium consisting of high-glucose Dulbecco's modified Eagle's medium (Gibco, USA) supplemented with 10 % fetal bovine serum (Gibco, UK) and 1 % penicillin/streptomycin (Gibco, USA). The material discs were stored in the culture medium for 24 h at 37 °C under 5 % CO₂. The ratio between the surface of sample discs and

Table 1
Components of experimental resin-based composites containing S-PRG filler.

	Composition (g)			S-PRG Filler content (wt%)
	Resin Matrix ^{a)}	Fine silica particles	S-PRG Filler	
G0	30.6	5.4	0.0	0.0
G10			4.0	10.0
G30			15.4	30.0
G50			36.0	50.0
G70			84.0	70.0
a) Resin Matrix Composition				
Composition				Content (wt%)
Bisphenol A-diglycidyl methacrylate (Bis-GMA)				69.7
Triethyleneglycol dimethacrylate (TEGDMA)				29.7
Comphorquinone (CQ)				0.3
1-Ethyl 4-(dimethylamino)benzoate (EDMAB)				0.3

the volume of medium was 1.5 cm²/mL. The extraction material medium was filtered through a 0.22 μm syringe filter (Merck Millipore) before use.

2.3. Characterization of material

The morphological structure and elemental distribution of the material surface (disc-shaped resin composites containing 0, 10, 30, 50, or 70 wt% S-PRG fillers) were determined with Scanning Electron Microscopy (SEM)–Energy-Dispersive Spectrometer (EDS) (Sigma 300, Zeiss, Germany). The elemental composition was evaluated by EDS analysis and X-ray Photoelectron Spectroscopy (XPS; Thermo Scientific K-Alpha, USA).

2.4. Physicochemical properties

The mechanical properties including flexural strength (FS), flexural modulus (FM), and compressive strength (CS) were tested using a universal testing machine (LLOYD EZ20, USA). Three specimens from each group were tested. According to ISO 4049-2019, all the material specimens were measured with 1.0 mm/min loading rate. The detailed calculation of FS, FM, and CS used the formulas: (1) $FS = 3Fl/2bh^2$, (2) $FM = Fl^3/4bh^3d$, (3) $CS = 4F/\pi D^2$, where F (N) is the maximum load, l (mm) is the length between the supporting span, b (mm) is the width of the specimen, h (mm) is the height of the specimen, d (mm) is the deflection under maximum load, and D (mm) is the diameter of the specimen.

Besides, water sorption of resin composites was detected. According to ISO 4049-2019, S-PRG-filling resin specimens and FZ specimens (Φ 15 mm × 1 mm) were dried at 37 °C for 22 h. Then, the procedure was repeated until the mass was constant. To record the volume (mm³), the accurate diameter and thickness of specimens were measured using a vernier caliper (to an accuracy of ±0.01 mm). All samples were immersed in deionized water at 37 °C. At different time points of 1, 7, 14, and 28 days, the immersed samples were taken out, dried, and weighed to record the mass (m1). Then, the above drying procedure was repeated until a constant mass (m2) was obtained. The water absorption (W_{sp}) was defined as: $W_{sp} = (m1-m2)/V$, where V is the volume of the specimen (mm³). Surface hydrophilicity was determined from the water contact angle, determined with a water contact angle instrument (Sunzern, China). Distilled water (4 μL) was dropped onto the material surface. After 2 s, the shape of the water drop was captured with a camera. Three specimens from each group were tested, and the mean value of the contact angle was calculated.

2.5. Ions release behavior and pH measurements

The disc-shaped S-PRG-filling resin specimens (including G0, G10, G30, G50, and G70) and FZ specimens (Φ 15 mm × 1 mm) was used to detect the ions release behavior. Each disc was individually immersed in 5 mL of deionized water for 7 days at 37 °C. Then, the solutions were collected at the time point and used to analyze the released concentration. The release of B, Na, Al, and Sr ions was determined with Inductively Coupled Plasma Optical Emission Spectrometer (ICP-OES; Agilent 5110, USA). The emission of F was measured with Ion Chromatography (IC; Aquion™ RFIC™ Ion Chromatography System, Thermo Fisher Scientific, USA). Three specimens from each group were tested. The effects of S-PRG on the environmental pH were determined with a pH meter (Sartorius, Germany), after the pH electrodes were calibrated with standard solutions at pH 4, 7, and 10 (Sangon Biotech, China). Three specimens were prepared for each group, and the mean pH was calculated after 0, 3, 6, 12, 24, and 48 h.

2.6. Cell culture

The study was approved by the Ethics Committee of the School of

Medicine, Shanghai Ninth People's Hospital Affiliated to Shanghai Jiao Tong University, China (Document No. 201769). Healthy and intact third molars were collected from individuals (18–22 years old) in the Ninth People's Hospital. The gingivae were removed, and the periodontal ligaments were digested in 3 mg/mL collagenase type I (Bioxon, Germany) for 1 h at 37 °C. The hPDLSCs were cultured with complete medium at 37 °C under 5 % CO₂. Cells taken from the cultures between the second and fifth passages were used for the subsequent experiments. To induce osteogenesis, hPDLSCs were subcultured in osteogenic induction medium (OM; Cyagen Biosciences, USA) containing L-ascorbic acid, dexamethasone, and β-glycerophosphate for up to 21 days.

2.7. Cytocompatibility

The hPDLSCs were cocultured with material discs. Cell Counting Kit-8 (CCK-8; Dojindo Laboratories, Japan) was used to evaluate cell viability. After 1, 3, and 7 days in culture, the medium was replaced with fresh medium containing 10 % CCK-8 solution, and then incubated for 1 h at 37 °C under 5 % CO₂. The optical density was measured at a wavelength of 450 nm (OD₄₅₀) with a microplate reader (Bio-Tek, USA). Live/dead staining was performed with the Calcein/PI Viability/Cytotoxicity Assay Kit (Beyotime, China) after 4 days in coculture. The samples were observed with fluorescence microscopy (Leica, Germany).

To observe cell adhesion on the material discs, hPDLSCs were seeded on the discs, cultured for 24 h, and fixed with 4 % paraformaldehyde (PFA; Sangon Biotech, China) for 30 min. The morphology of the hPDLSCs was visualized with immunofluorescent staining and SEM. After the cells were fixed, phalloidin (Yeasen Biotech, China) was used to stain the cytoskeleton and 4',6-diamidino-2-phenylindole (DAPI; Beyotime) to stain the nuclei. Images were captured with a confocal laser scanning microscope (Zeiss). Similarly, cells were fixed with fixation solution (Servicebio, China) on ice for 2 h, after which the samples viewed with SEM (Zeiss Sigma 300).

2.8. RNA isolation and determination

The effects of S-PRG on osteogenesis and angiogenesis were analyzed with reverse transcription (RT)–quantitative PCR (qPCR) to evaluate the levels of mRNA expression. Total RNA was extracted from hPDLSCs with TRIzol Reagent (Invitrogen, USA). The PrimeScript RT reagent Kit (Takara, Japan) was used for reverse transcription. Gene transcription levels were quantified with PCR using TB Green Premix Ex Taq (Takara, Japan) on a LightCycler 480 II instrument (Roche, Switzerland), and calculated with the 2^{-ΔΔCt} method. The primers for the target genes are listed in Table 2.

2.9. Osteogenic experiments

HPDLSCs were plated in 12-well plates (2 × 10⁴ cells per well) and cultured with the material discs in OM for 4 days. The cells were washed twice with phosphate-buffered saline (PBS) and fixed with 4 % PFA solution for 30 min. Staining for alkaline phosphatase (ALP) was performed according to the manufacturer's instructions (Beyotime). The ALP activity was measured using Alkaline Phosphatase Assay Kit (Beyotime). Cells were stained with Alizarin Red S (ARS) to detect

mineralization after they were cultured with material discs in OM for 21 days. After the cells were washed twice with PBS and fixed, ARS solution (Beyotime) was added to visualize calcium deposition. The cells were incubated for 15 min at room temperature and washed to stop the reaction. Images were taken under an optical microscope.

2.10. Cell migration

A wound healing assay and Transwell assay were conducted to evaluate the cell migration induced by S-PRG. HPDLSCs were seeded onto the material surfaces and left to proliferate. When the cells reached 90 % confluence, a scratch wound was created with a sterilized 200 μL pipette tip. The plates were washed three times with PBS to remove any remaining cell debris. After 0 and 24 h, the cells on the material discs were fixed with 4 % PFA and stained with the crystal violet staining solution (Beyotime). Images of the healing wounds were captured under a microscope (Leica Microsystems, Germany). A Transwell plate (Corning, USA) was used to assess the vertical migration of the cells. The material discs were placed in the lower chamber, and 200 μL of hPDLSC suspension (3 × 10⁵ cells per mL) was added to the upper chamber and cultured for 24 h. After the cells were fixed, crystal violet staining solution (Beyotime) was used to stain them before observation under a microscope. The results were quantified using Image J analysis.

2.11. Analysis of angiogenesis

Vascular endothelial growth factor A (VEGFA) is an important protein in vascular development. The expression of VEGFA was visualized with immunofluorescent staining with a primary antibody directed against VEGFA (1:200; Zen BioScience, China). The tube formation induced by S-PRG was also measured. Matrigel (100 μL; Corning) was added to each well of a 48-well plate and allowed to gel for 30 min. Human umbilical endothelial cells (HUVECs; 5 × 10⁴ cells per well) were seeded in each well in material extraction medium. After incubation for 6 h at 37 °C under 5 % CO₂, the plate was observed with an optical microscope. The results were analyzed with the Image J V1.8.0.

2.12. Animal model construction and Masson trichrome staining

All animal procedures were approved by the Animal Care and Use Ethics Committee of Shanghai Ninth People's Hospital, Shanghai Jiao Tong University (Document No. SH9H-2024-A1036-1). To investigate the application of S-PRG-containing resin *in vivo*, a subgingival defect model in eight-week-old Sprague Dawley rats (bodyweight, 350–400 g) was constructed. Two commercial dentistry materials were selected to fill the subgingival defects. Beautiful Flow Plus X (F00) (Shofu Inc.), a flowable resin containing 67.3 wt% S-PRG, is a commercial dentistry material used in clinical practice. It was selected to fill the subgingival defects in S-PRG group to verify the effectiveness of S-PRG filling, while another commercial resin material served as the positive control (denoted as FZ). The rats were randomly divided into five groups: control group, sham operation group, subgingival defect group, S-PRG group, and FZ group. The animals were anesthetized before surgery. Following flap surgery at the palatal gingiva of the upper first molar, a subgingival defect was created with a round dental bur and then filled with resin materials. The rats were killed 3 weeks after surgery and their

Table 2
Primer sequences used in RT-qPCR.

Genes	Forward primer (5'–3')	Reverse primer (5'–3')
ALP	ACTGGTACTCAGACAACGAGAT	ACGTCAATGTCCTGATGTTATG
RUNX2	TCAACGATCTGAGATTTGTGGG	GGGGAGGATTTGTGAAGACGG
COL1A	GAGGGCCAAGACGAAGACATC	CAGATCACGTCATCGCACAAAC
VEGFA	AGGGAAGAGGAGGATGAG	GCTGGGTTTGTCCGGTGT
ACTB	CCACGAAACTACTCTCAACTCCATC	AGTGATCTCCTTCTGCATCTCTGTC

mandibles harvested and fixed in 4 % PFA for 48 h. Masson trichrome staining was performed to observe the reconstruction of the periodontal tissue and its adhesion to the resin surface.

2.13. Statistical analysis

All experiments were performed with a minimum of $n = 3$ samples per group. Statistical analyses were performed with the GraphPad Prism 8.0.2 software (GraphPad, USA) and are presented as means \pm standard deviations (SD). The normal distribution of the data was confirmed with Q-Q plots. All data were analyzed statistically with one-way ANOVA followed by Tukey's multiple-comparisons test. For all statistical tests, data were provided as means \pm SD. $P < 0.05$ was considered statistically significant.

3. Results and discussion

3.1. Characterization of S-PRG-filled resin composites

To explore the restorative treatment suitable for subgingival dental defects, S-PRG fillers were incorporated experimentally into resin composites (Figs. S1 and A). To determine their superficial microstructure and elemental distributions, S-PRG-filling resin composites (including G0, G10, G30, G50, and G70) were selected for an SEM-EDS analysis. As shown in Fig. 2A, some unfilled valleys were observed on the surfaces of G0. The superficial density of the particles increased as

the S-PRG filler content increased, indicating that the fillers were evenly spread onto the material. The particles almost covered the entire surface of the disc when the content of the S-PRG filler was 70 wt%. Subsequently, the composition of disc-shaped materials was analyzed. The corresponding EDS spectra (Fig. S2) showed that the peaks of the O, F, Na, Al, Si, and Sr elements increased as the S-PRG content increased. According to the weights and atomic contents of elements analyzed by EDS in Fig. 2B, G0 and G70 were selected for further detection of element distribution. The results of elemental mapping showed that G70 contained a higher amount of F, Sr, Na, and Al elements, which exhibited a uniform distribution on the surface (Fig. 2C). Consistently, compared with the XPS spectrum of G0, higher peaks of F, Sr, Na, and Al elements were observed in G70 samples (Fig. 2D). Among the four elements analyzed, the binding energy of Sr 3d was located at 134.38 and 135.88 eV for SrF_2 (about 69.93 %) and SrO respectively in G70. Collectively, resin composite discs containing homogeneously deposited S-PRG filler were successfully fabricated.

Sufficient mechanical strength of resin-based materials is important for dental restoration [27]. As shown in Fig. 3A, the FS of all specimens was greater than 80 MPa, complying with the basic requirement for mechanical properties according to ISO 4049-2019. Comparing the S-PRG-filling resin composites to FZ group, the FS value was significantly decreased when the S-PRG filler content reached 30 wt%, which was consistent with previous study [28,29]. The decreased FS might contribute to the fact that higher filler content hindered the interfacial interactions and attenuated the involvement of polymer chains in resin

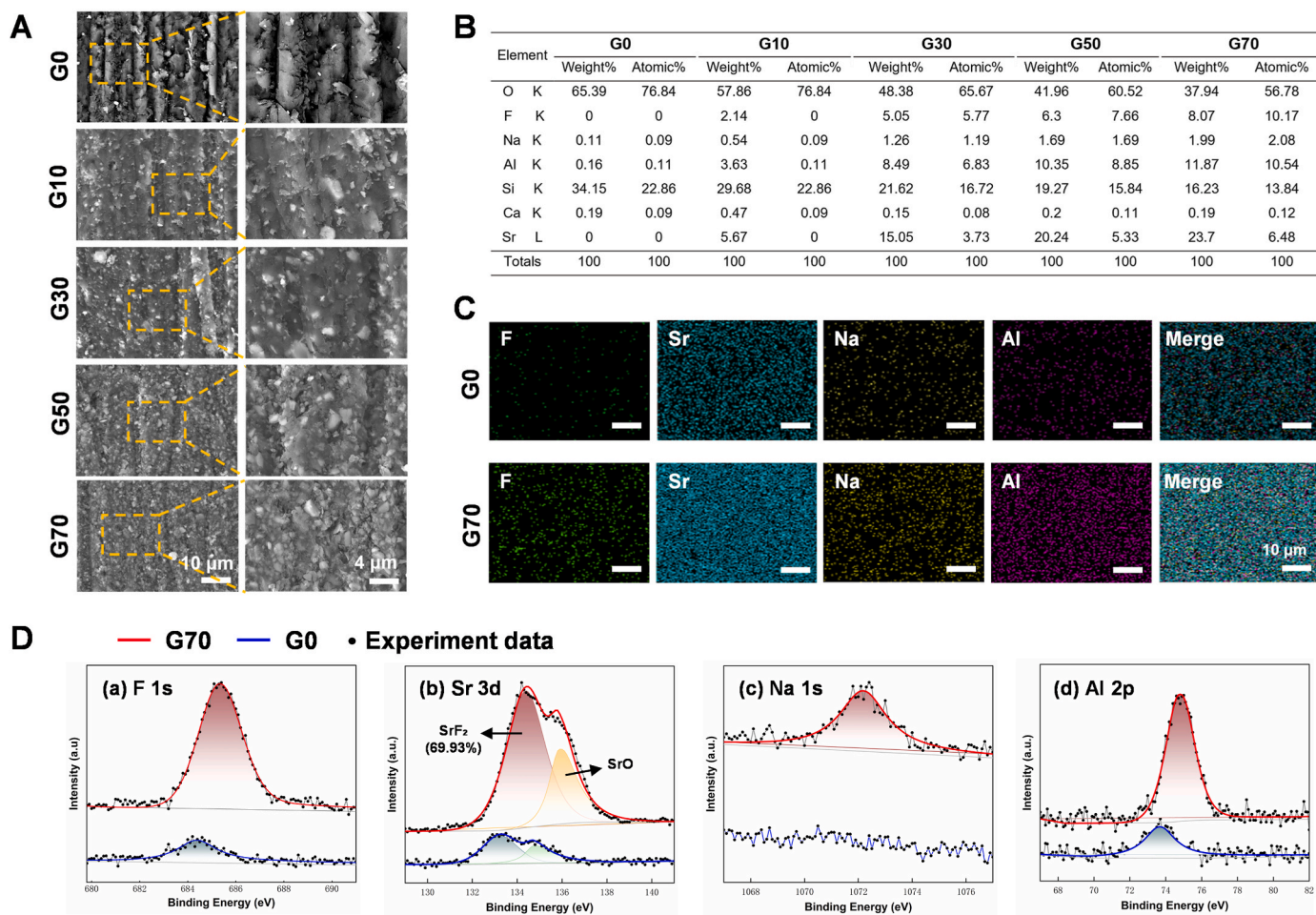


Fig. 2. Morphological structure and elemental distribution of material discs containing S-PRG filler. (A) Morphology of material surface (containing 0, 10, 30, 50, or 70 wt% S-PRG filler) determined with SEM. (B) List of elements distributed on the surface of the material, according to weight and atomic percentages. (C) Elemental mapping of G0 and G70 (scale bar: 10 μm). (D) XPS spectra of F, Sr, Na, and Al elements in G0 and G70.

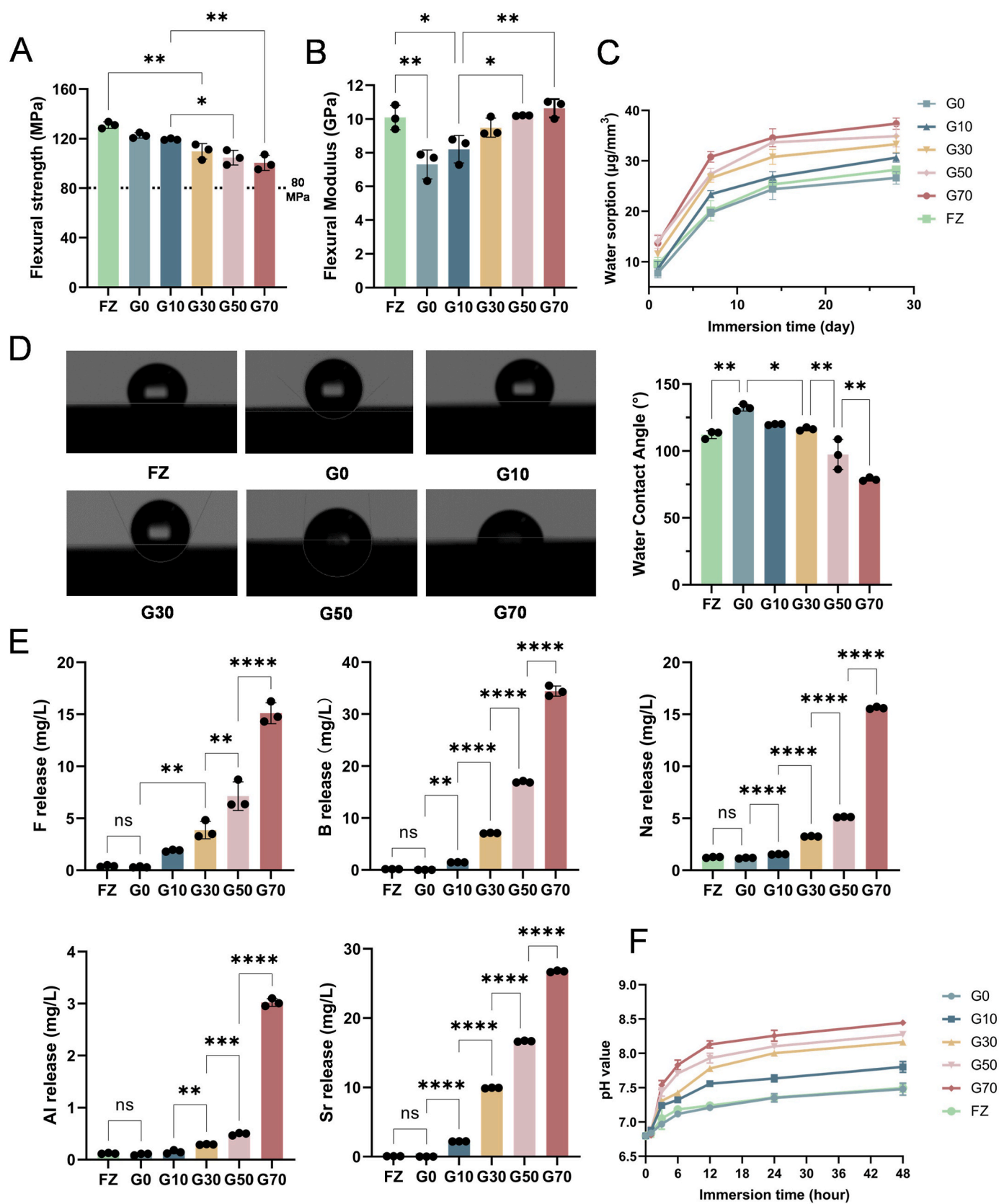


Fig. 3. The physicochemical properties of material discs. (A) Flexural strength, (B) Flexural modulus, (C) Water sorption, and (D) Water contact angles of FZ, G0, G10, G30, G50, and G70. (E) Ions released after the material discs were immersed in deionized water for 7 days, determined by inductively coupled plasma and ion chromatography. (F) pH measured after immersion of discs for 0, 3, 6, 12, 24, and 48 h. The results are expressed as mean \pm SD (ns, no significance; * $P < 0.05$, ** $P < 0.01$, *** $P < 0.001$, and **** $P < 0.0001$).

matrix [30]. Meanwhile, the FM was significantly relevant to S-PRG filler content (Fig. 3B). The FM of G70 (10.64 ± 0.5495 GPa) was higher than other S-PRG containing groups, showing no significant difference from FZ. In addition, as shown in Fig. S3, the CS value of G50 (305.6 ± 1.481 MPa) and G70 (301.7 ± 2.364 MPa) was closer to the CS of dentin tissue (297.17 MPa) [31]. Based on the results above, all the experimental resin composites possessed a certain mechanical strength, while G50 and G70 exhibited comprehensively better mechanical properties than other groups.

The water sorption of S-PRG-filling resin composites and FZ group complied with the standard of ISO 4049-2019, which were below $40 \mu\text{g}/\text{mm}^3$ after immersion in water for 7 days (Fig. 3C). The increased water sorption with increased S-PRG filler content might contribute to higher resin hydrophilicity and possibly promote the ion release from S-PRG filler through the resin matrix [30,32]. The surface hydrophilicity of a biomaterial is considered to influence cellular adhesion to it [33]. Therefore, we tested the water contact angles on the six types of material discs. As shown in Fig. 3D, the water contact angle on the sample discs without S-PRG was $132.3^\circ \pm 2.568^\circ$, which decreased to $112.3^\circ \pm 2.928^\circ$ on FZ discs, to $116.5^\circ \pm 1.283^\circ$ on G30 discs, to $97.4^\circ \pm 11.26^\circ$ on G50 discs, and to $78.81^\circ \pm 1.339^\circ$ on G70 discs. A significant reduction was observed in discs with 70 wt% S-PRG, suggesting that a high concentration of S-PRG increases the cytocompatibility of the resin-based composites. The increase in surface hydrophilicity induced by the SPGR filler improved the likelihood of cell adhesion and proliferation.

3.2. Ion release profile and pH measurements of S-PRG-filling resin composites

The glass ionomer phase of S-PRG fillers serves as a reservoir of multi-ions. Owing to this unique structure, S-PRG fillers can characteristically release multiple ions, which may contribute to the bioactive functions of S-PRG. The release of Al, Na, Sr, B, and F ions was detected after the disc-shaped resin samples were immersed in deionized water for 7 days. The results shown in Fig. 3E indicate a significant S-PRG-concentration-dependent increase in the release of five ions. In the group of S-PRG-filling resin composites (G0, G10, G30, G50, and G70), the ion release of Na, Sr, F, and B increase markedly with higher S-PRG filler content, while the Al ion concentration remains relatively low. By contrast, FZ specimens show little compatibility of ion release. The increases in ion release may be attributable to the presence of the pre-reacted glass-ionomer phase and the fluoroboroaluminosilicate glass core [19,34,35]. More importantly, certain amounts of F are considered essential for the development of bone and teeth. Fluorine stimulates osteogenesis by inducing the proliferation and activity of osteoblasts, and the co-incorporation of F and Sr is reported to enhance cellular proliferation and promote osteogenesis [36,37]. Besides, multiple ions might interfere with the biological activity of some bacteria. In previous studies, S-PRG fillers have been reported to inhibit bacterial growth and acid production of *Streptococcus mutans*, and the effects mainly contributed to the release of B and F ions [21]. Hence, the structural characteristics of the S-PRG filler determined the capacity of the S-PRG-containing resin to release biofunctional ions, which may play a role in tissue regeneration.

The modulatory effect of the S-PRG filler on the acidity of the environment was investigated with pH measurements (Fig. 3F). The pH values were recorded at 0, 3, 6, 12, 24, and 48 h. The pH clearly increased rapidly, within the initial 12 h, under the influence of the S-PRG filler, whereas the increase in pH was mild and stable during the period from 12 h to 48 h. The results demonstrated that S-PRG fillers could modulate the pH of surrounding medium towards a weak alkaline environment. Consistently, in previous studies, S-PRG-filling restorative materials have been observed to provide a pH neutralization capacity and preserve the demineralization of enamel surface. The mechanism of how the ions released from S-PRG inhibited enamel demineralization

remained unclear [38,39]. However, the released ions of Sr and Na from S-PRG were considered to possibly promote acid buffering [19]. Therefore, the pH modulation capacity of S-PRG-containing resin composites, possibly contributing to the multiple ions released, might provide a protective effect against the demineralization process.

3.3. Cytocompatibility

The cytocompatibility of resin composite is important for cell adhesion and proliferation, so we tested whether the inclusion of the high-concentration S-PRG filler induced cytotoxicity in the composite resin. After 1, 3, and 7 days of cell culture with the resin discs, a CCK-8 assay was performed to investigate the cytotoxic effect of the filler on the attached cells. The results (Fig. 4A) showed adequate cell viability in all groups, which tended to increase throughout the culture period, implying that hPDLSCs could proliferate on the material discs. The OD^{450} values of G70 were significantly higher than those of the other resin composites on days 1 and 7 compared to the blank medium and FZ group, suggesting that high-concentration S-PRG filler promotes cell proliferation and increases cellular biocompatibility. This might contribute to the released fluorine ions, which were reported to favor cell proliferation [40]. The Live/dead staining was performed after 4 days of cell culture with a blank medium or resin discs. Fluorescence imaging (Fig. 4B) showed small, red-stained dead cells on the S-PRG-containing resin composites and FZ group. Obviously, none of the samples exhibited notable cytotoxicity compared to the blank medium. These results confirmed the satisfactory biocompatibility of the resin composites with different S-PRG filler contents.

Cell adhesion on biomaterials is crucial for the modulation of cellular function [41]. To evaluate the effect of the S-PRG filler on cell adhesion to S-PRG-containing resin, the cell morphology and cytoskeletons were visualized with SEM and cytoskeletal staining, respectively. HPDLSCs were stained with phalloidin–fluorescein isothiocyanate (green) and DAPI (blue) after 1 day of culture on the surfaces of the material discs. Confocal fluorescence imaging (Fig. 4C) showed that the cells adhering to the discs of G0 and FZ displayed a narrow spreading pattern and maintained a fibroblast-like morphology, whereas the cells on the S-PRG-containing material discs spread much more widely and adopted a polygonal shape as the proportion of S-PRG filler increased. The corresponding SEM images showed that filopodia extension was initially detected on G10 discs, whereas significant filopodia extending in various directions was observed on G50 discs. When the S-PRG content reached 70 wt%, the cells seemed to spread more extensively than in the other groups, with a polygonal spreading pattern. These morphological changes suggest strong cell adhesion to the material surface as the S-PRG filler content increased, which may be attributable to the release of bioactive ions from the S-PRG. In summary, no apparent cytotoxicity was detected for the five tested materials, and the resin composite with 70 wt% S-PRG filler showed excellent potential utility in terms of the cell adhesion to it and cellular proliferation on it, which should favor gingival adhesion and tissue regeneration during its practical application in resin filling.

3.4. Osteogenic differentiation

The capacity to promote osteogenesis is vital for resin material used in situations complicated with bone defects. Therefore, the ability of S-PRG filler to induce the osteogenic differentiation of hPDLSCs was investigated. Total RNA was extracted from hPDLSCs after 7 and 21 days in culture in OM with the material discs. The expression of osteogenic marker genes by the hPDLSCs, including *RUNX2*, *ALP*, and *COL1A*, was measured with RT–qPCR (Fig. 5A and B). Compared with the control group, the hPDLSCs treated with FZ, G50, or G70 discs showed higher early expression (7 days of culture) of *ALP* and *COL1A*. The expression of *RUNX2* mRNA did not differ significantly among the six types of resin in the initial stage of osteogenic induction. As shown in Fig. 5B, after 21

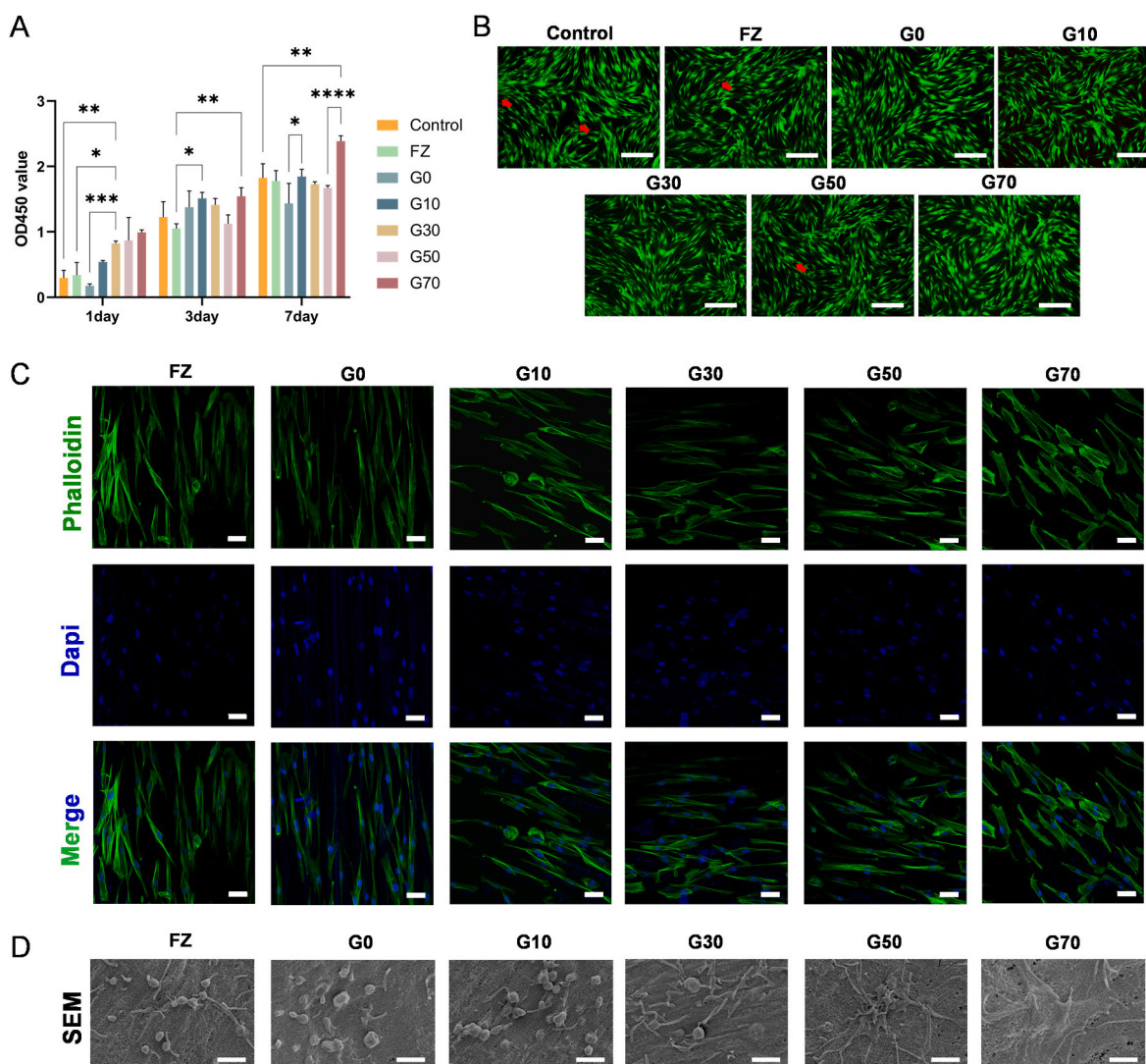


Fig. 4. Effects of S-PRG filler on cell biocompatibility. (A) Proliferation of hPDLSCs cultured with material discs for 1, 3, or 7 days, examined with CCK-8. (B) Living cells (green) and dead cells (red arrows) of hPDLSCs were cultured with material discs for 4 days (scale bar: 100 μm). (C) Cytoskeletons of hPDLSCs seeded on the surfaces of material discs for 24 h, stained with phalloidin (green) and DAPI (blue) (scale bar: 50 μm). (D) SEM images of hPDLSCs cultured on the surfaces of material discs (scale bar: 1 μm). The results are expressed as mean \pm SD (* P < 0.05, ** P < 0.01, *** P < 0.001, and **** P < 0.0001).

days in coculture, the transcription of all the osteogenic genes tested was increasingly upregulated as the SRPG filler content increased. *RUNX2* is a critical transcription effector of osteoblast differentiation, promoting the maturation of immature osteoblasts [42]. Although no significant changes were observed in its expression during early osteogenic induction, *RUNX2* showed significantly higher late expression in the cells adherent to resins containing 50 wt% and 70 wt% S-PRG filler. *COL1A*, encoding the main component of the bone matrix, showed an increasing trend throughout the period of osteogenic induction [43]. After 21 days in coculture, a low proportion of S-PRG filler (30 wt%) caused an obvious increase in *COL1A* gene expression, whereas 70 wt% S-PRG filler increased *COL1A* expression approximately 10-fold relative to the control group. Therefore, the qPCR results demonstrated that the S-PRG filler promoted osteogenic differentiation in hPDLSCs, benefitting bone reconstruction. Comprehensively, G70 exhibited the best improvement of the mRNA expression of osteogenic marker genes compared to other groups.

ALP is considered an essential factor modulating the biochemical mineralization of hard tissues, such as bone and cartilage, which functions in the early stage of osteoblast differentiation and promotes bone matrix formation [44–46]. Corresponding to the qPCR results for *ALP*,

the stained images shown in Fig. 5C demonstrate the marked S-PRG-content-dependent increasing trend in ALP. The ALP activity in the hPDLSCs was evaluated after 4 days of osteogenic induction (Fig. 5D). An obvious increase in ALP activity was observed when the content of S-PRG filler was 50 wt%, suggesting that the presence of S-PRG facilitates mineralization and bone formation. Similar results were observed, with the same trends, after ARS staining (Fig. 5E). After osteogenic induction for 21 days, greater formation of mineralized calcium nodules was observed in the cells cocultured with material discs containing S-PRG filler, especially with the resin containing 70 wt% S-PRG. Overall, the presence of S-PRG filler increased osteogenic differentiation and bone formation compared with that in the control group, which may be attributable to the ions released by S-PRG fillers [47–49]. Among the multiple ions released from S-PRG fillers, Sr and F are known as excellent osteogenic factors [50]. F possesses a strong affinity for bone tissue and modulates bone turnover process. Low-dose F can increase bone formation via stimulating the proliferation of osteoblasts [51,52]. Analogously, Sr^{2+} is also one of the trace elements in the human body related to bone metabolism. It has been demonstrated that Sr^{2+} can increase bone formation by activating the osteoblasts and reduce bone resorption through inhibiting the osteoclast activity in the

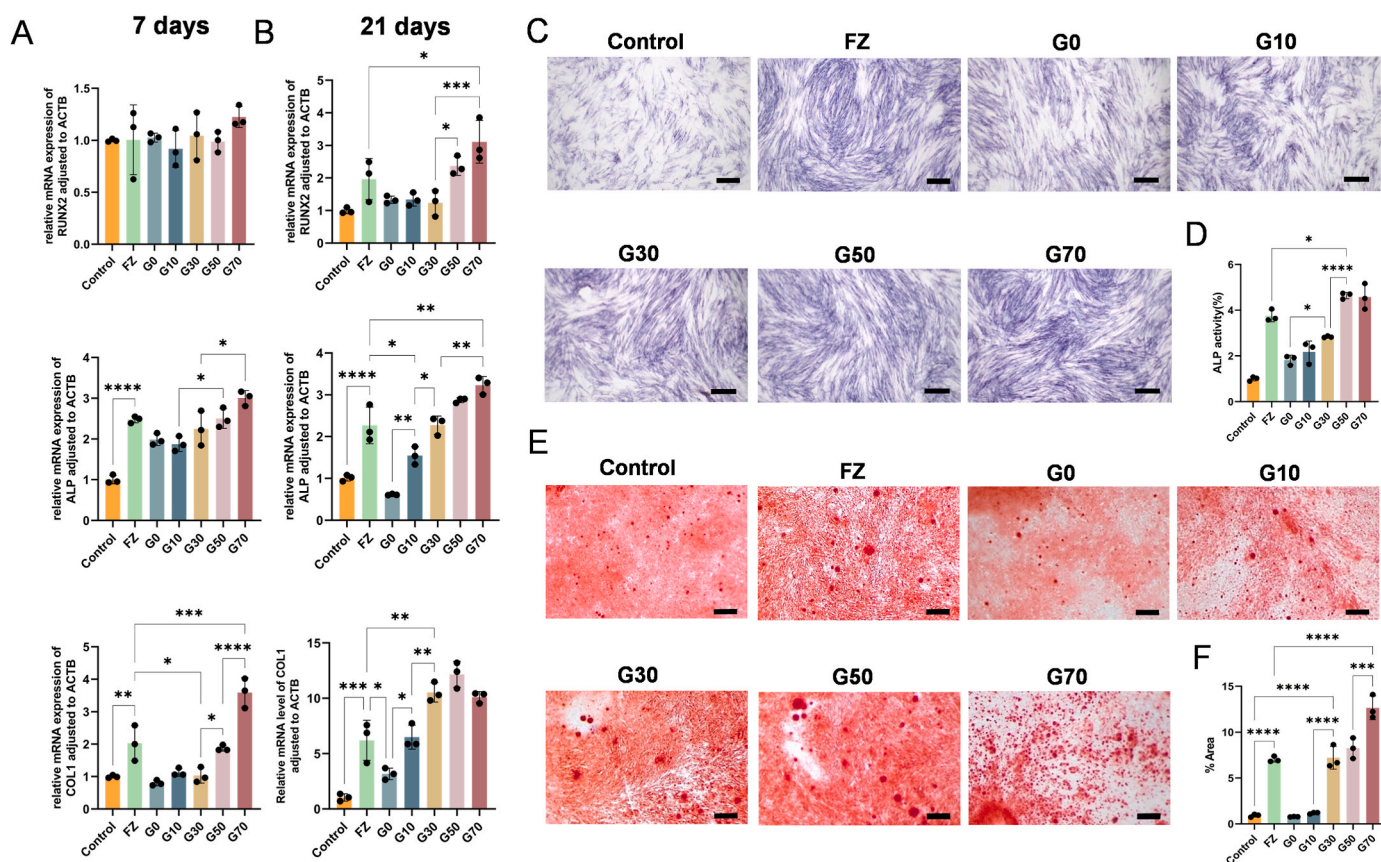


Fig. 5. Effects of S-PRG filler in regulating osteogenesis. (A) Expression of genes *RUNX2*, *ALP*, and *COL1A1* after cells were cultured with material discs for 7 days or (B) 21 days. (C) Staining of hPDLSCs for ALP after 4 days in culture with material discs (scale bar: 1 mm). (D) Quantitative analysis of ALP activity in (C). (E) ARS staining of hPDLSCs cultured with material discs for 21 days (scale bar: 1 mm). (F) Quantitative calculation of ARS-stained areas in (E). The results are expressed as mean \pm SD (* P < 0.05, ** P < 0.01, *** P < 0.001, and **** P < 0.0001).

meantime [53]. Mechanically, Sr^{2+} promotes the osteogenic differentiation of mesenchymal stem cells by upregulating the osteogenic marker genes, including *RUNX2*, *ALP*, *OPN*, and so on. The signaling pathways like *Wnt*/ β -Catenin were considered to be activated in Sr^{2+} induced osteogenesis [54,55]. Moreover, Sr^{2+} also plays a promoter during the angiogenic procedure [56]. Boron is also involved in bone health modulation by preventing calcium loss and demineralization [52]. Hence, the excellent cytocompatibility and osteogenic properties of resin composites containing high proportions of S-PRG filler indicate their potential utility in complex dental treatments in the clinical context.

3.5. Angiogenic experiments

Angiogenesis is considered to collaborate with osteogenesis during bone repair. Cell proliferation and migration are essential for angiogenesis [57]. Consequently, the effect of S-PRG on angiogenesis was investigated *in vitro*. First, the horizontal migration of hPDLSCs was assessed with a wound healing assay (Fig. 6A). To mimic the cell migration on the resins, the cells were directly seeded onto the material surfaces and allowed to proliferate for 24 h. The cells seeded on the surface of FZ, G0, and G10 disc showed extremely low levels of cell migration. This suggested that FZ and low concentrations of S-PRG have little effect on cell migration. However, when the concentration of S-PRG filler was 30 wt%, wound closure area was markedly smaller than in the G0 and decreased as the S-PRG content increased. The vertical migration of hPDLSCs was evaluated in a Transwell experiment (Fig. 6B). More cells were transferred to the other side of the Transwell membrane in response to S-PRG-containing resin, especially that with

higher S-PRG content of 30–70 wt%. Compared with the FZ and G0, the number of migrated cells per field increased about four-fold when the S-PRG content was 50 % (Fig. 6C). In conclusion, high concentrations of S-PRG filler in resin composites facilitate cell migration in both vertical and horizontal directions, which demonstrates the potential of S-PRG to promote gingival adhesion to the restorative material during the treatment of subgingival defects.

VEGFA is an angiogenesis-associated protein that promotes vascular development. Therefore, the level of VEGFA was investigated *in vitro* to determine the modulation of angiogenesis by S-PRG [58]. Total RNA was harvested from cells after their culture with material discs for 24 h. A quantitative analysis indicated that the expression of *VEGFA* mRNA in cells adherent to composite resin containing 50 wt% or 70 wt% S-PRG filler was significantly elevated, two- and three-fold, respectively (Fig. 6D). Immunofluorescent staining was used to visualize the expression of VEGFA, which showed the same increasing trend. Markedly enhanced fluorescence intensity was observed in cells cultured with resin containing 70 wt% S-PRG filler, with an approximately two-fold increase in intensity (Fig. 6F). Representative images are presented in Fig. 6E. A subsequent tube-forming assay with HUVECs was conducted to quantify the vascularization induced by S-PRG (Fig. 6H). During cell culture with material extraction medium, the formation of tubes, nodes, and branches was clearly observed after 6 h. Quantification of the junctions, branches, and total lengths of the tubes is shown in Fig. 6G and indicated that high-concentration S-PRG filler has satisfactory angiogenic properties.

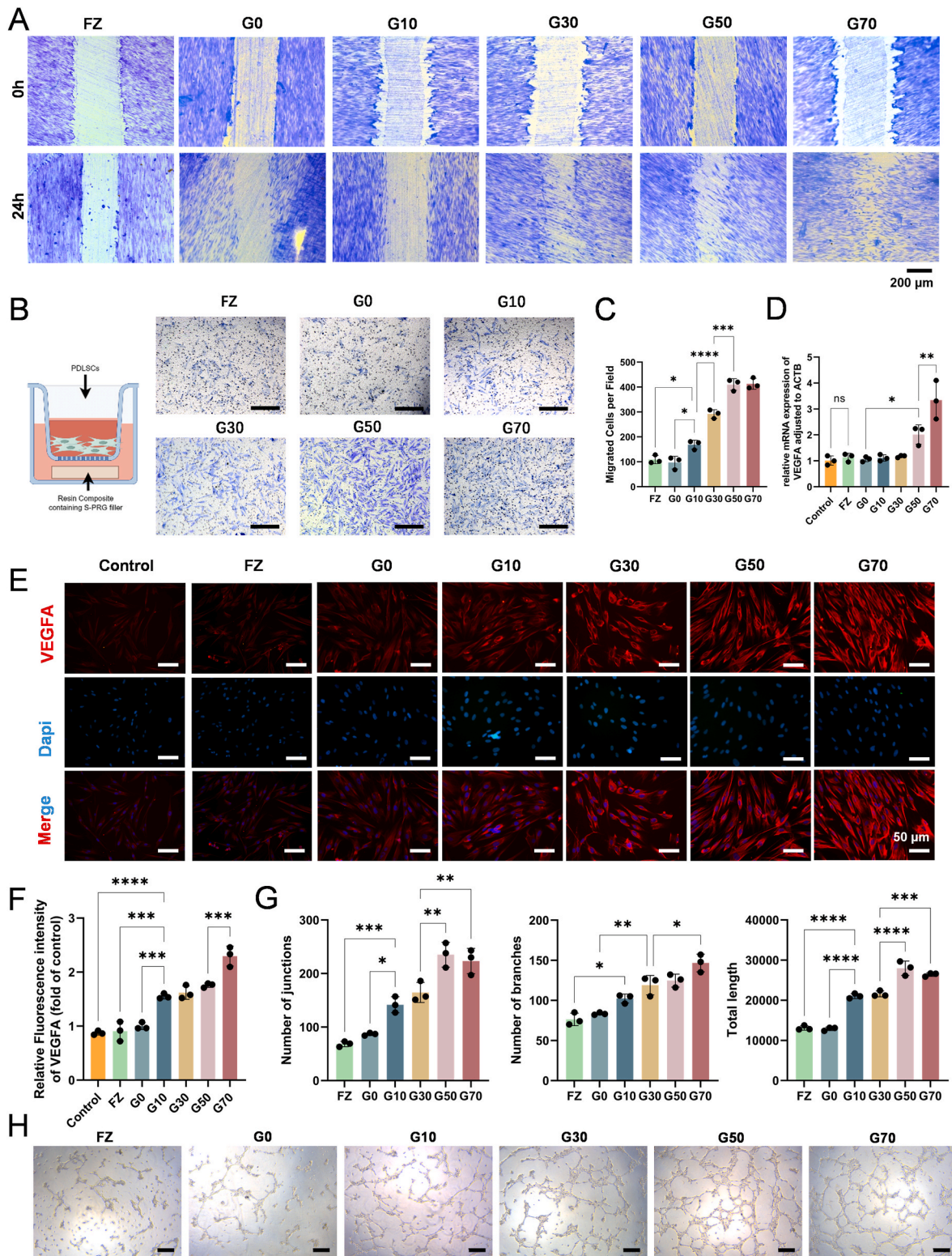


Fig. 6. Angiogenic effects induced by S-PRG filler *in vitro*. (A) Wound healing assay (scale bar: 200 μ m). (B) Transwell assay was used to evaluate the vertical migration of hPDLSCs (scale bar: 100 μ m), (C) Quantitative analysis of migrated cells per field. (D) Expression of VEGFA gene in hPDLSCs cultured with material discs for 24 h. (E) Immunofluorescent staining of hPDLSCs: red (VEGFA) and blue (DAPI) (scale bar: 50 μ m). (F) Quantitative calculation of fluorescence intensity of VEGFA in (E). (G-H) Tube-forming assay (scale bar: 200 μ m) and quantitative analysis: number of junctions, number of branches, and total length. The results are expressed as mean \pm SD (ns, no significance; * P < 0.05, ** P < 0.01, *** P < 0.001, and **** P < 0.0001).

3.6. Application of S-PRG-containing resin composites to subgingival defects *in vivo*

The results described above suggest that high-concentration S-PRG filler endows resin composites with excellent abilities to prompt cell proliferation, cell adhesion, osteogenesis, cell migration, and angiogenesis. The properties shown by S-PRG may be attributed to its structural characteristics and indicate its possible utility in restoring subgingival defects. It is noteworthy that 50–70 wt% S-PRG filler

showed greater biological activity than the low-S-PRG-concentration resins. Beautifil Flow Plus X (F00) is a commercial dentistry material used clinically that contains 67.3 wt% S-PRG filler. To evaluate the effectiveness of S-PRG, Beautifil Flow Plus X (F00) was used to fill subgingival defects in rats. Meanwhile, a commercial resin material commonly used in clinical settings served as a positive control group. Eight-week-old Sprague Dawley rats were randomly divided into five groups: the control (normal rats); sham-operated (only flap surgery was performed on the rats); subgingival defect (defects were created, but not

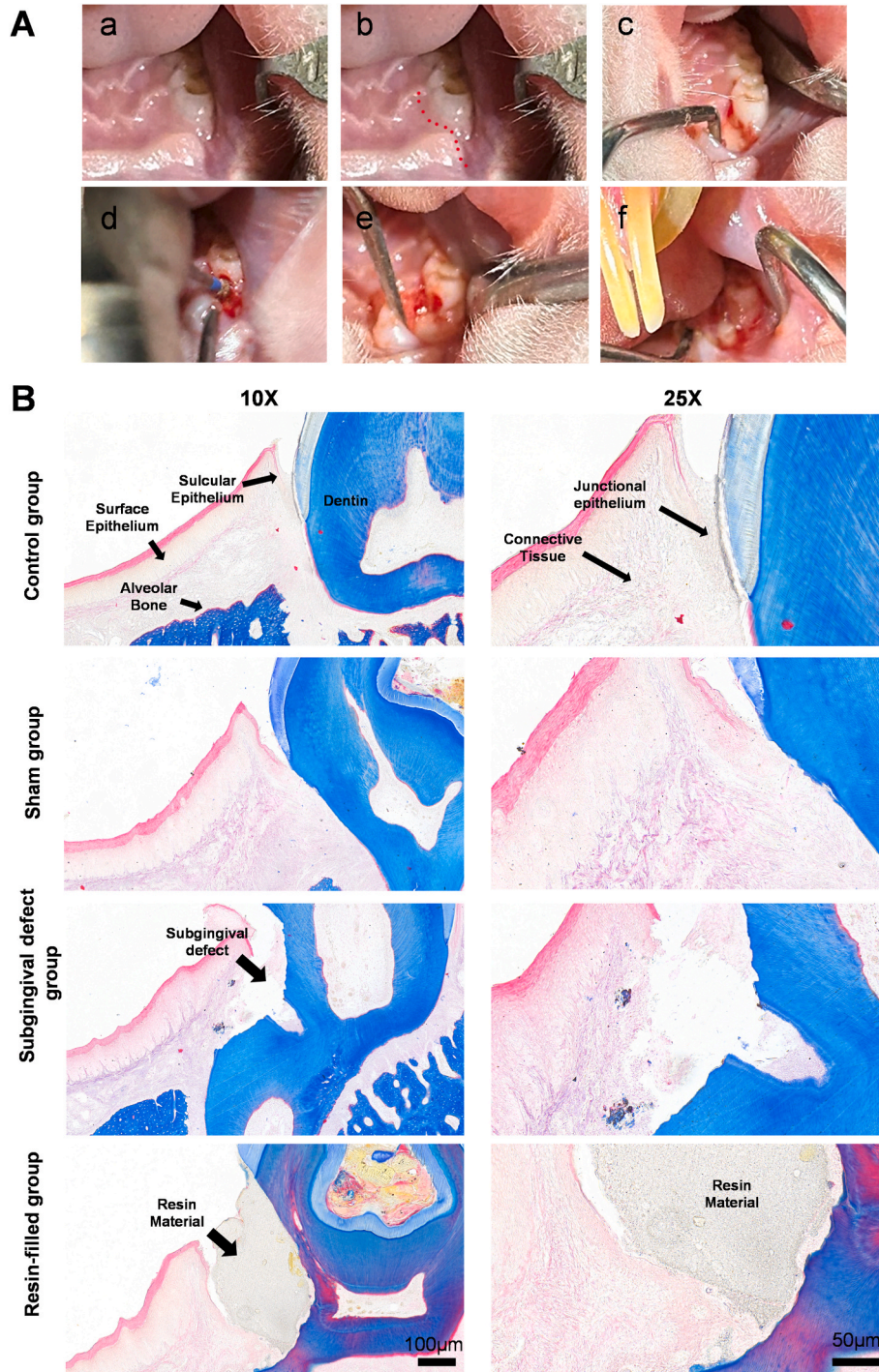


Fig. 7. Application of flowable resin composites containing S-PRG to subgingival dental defects *in vivo*. (A) Procedures of the operation. a) Rats were anesthetized and the surgical fields of the maxillary first molar were exposed. b) Surgical incision was made on the palatal side of the gingiva. c) Flap surgery was performed. d–e) A subgingival dental defect was created with a round dental bur at the cemento–enamel junction. f) S-PRG-contained flowable resin was used to fill the subgingival defect. (B) Representative Masson trichrome staining of the tooth and periodontal tissue at 3 weeks after surgery.

be filled); S-PRG group (defects were created and filled with flowable resin containing S-PRG constituents); FZ group (defects were filled with a commercial flowable resin material). The key steps in the surgical procedures are recorded in Fig. 7A.

To examine tissue healing, the teeth and surrounding periodontal tissues were stained with Masson trichrome. The results are presented in Fig. 7B. In the control group, the dentin and gum structures are clearly visible. In the physiological condition, the sulcular epithelium is intact, and the junctional epithelium adheres to the enamel towards the root apex. The rats in the sham group only underwent flap surgery. The results showed that the structure of periodontal tissues had almost recovered by 21 days, suggesting that flap surgery had little effect on tissue recovery. However, in the subgingival defect group, the overall structure of the periodontal tissue was injured. In the presence of the subgingival defect, the epithelial structure surrounding the teeth was damaged. The absence of a dento-gingival junction, which is mediated by the junctional epithelium, destroyed the interface between the teeth and the periodontal tissue. The destruction of the defense system probably caused the regional necrosis of the nearby epithelium and connective tissue. By contrast, with the application of S-PRG-containing flowable resin composite, the epithelial structure was visible and intact. More interestingly, the periodontal connective tissue below the epithelial layer seems to adhere to the resin material surface. No obvious sign of inflammation was detected surrounding the resin material, suggesting that the biocompatibility of the resin enhanced tissue recovery. In FZ group displayed in Fig. S4, the epithelial structure was also visible and intact, suggesting that both commercial resin composites have favorable biocompatibility. However, no obvious gingival adhesion to the resin surface was observed in the positive control group. It suggested that S-PRG-filling resin composites might be favorable for gingival recovery against the subgingival defects. The results demonstrate the feasible application of high-concentration S-PRG to the treatment of subgingival defects in an animal model.

4. Conclusion

In this study, an S-PRG filler composed of three layers was fabricated and incorporated into resin-based composites. The characteristic structure of the prereacted glass-ionomer phase may have contributed to the biofunctions shown by S-PRG. The filler was evenly embedded within the resin composite to direct the properties of the material surface. Increasing the S-PRG content increased the abundance of the surface elemental distribution and the surface hydrophilicity. The material solution also discovered an improved efficiency of ion release and pH regulation. HPDLSCs seeded on the material surface spread more extensively and adopted an increasingly polygonal shape as the S-PRG content increased. The ability to change the cell morphology indicates that S-PRG facilitates hPDLSC proliferation, adhesion, and osteogenic differentiation. This was confirmed by the upregulated expression of osteogenic marker genes (*RUNX2*, *COL1A*, and *ALP*), enhanced ALP activity, and the increased production of mineralized calcium nodules. Given the relationship between osteogenesis and angiogenesis, the biocompatibility of S-PRG with cell migration and tube formation was confirmed. More importantly, the S-PRG-containing resin was successfully applied to subgingival defects, with favorable restoration and adhesion to the periodontal tissue, indicating its suitability for the treatment of deep dental caries or fractures involving subgingival defects. In this study, we introduced resin composites incorporating bioactive particles of S-PRG, and demonstrated their biocompatibility, thus providing an alternative material for the restoration of subgingival dental defects in the clinical context.

CRediT authorship contribution statement

Yueyi Yang: Writing – original draft, Methodology, Investigation, Formal analysis, Data curation. **Jing Huang:** Validation, Software, Data

curation. **Xuchen Hu:** Validation, Software, Resources. **Meiling Jing:** Supervision, Project administration, Conceptualization. **Yujie Zhang:** Resources, Investigation. **Chenci Xu:** Project administration, Investigation. **Wenduo Tan:** Software, Investigation, Conceptualization. **Xiaoyu Liu:** Resources, Investigation. **Chenguang Niu:** Writing – review & editing, Writing – original draft, Methodology, Funding acquisition. **Zhengwei Huang:** Writing – review & editing, Writing – original draft, Project administration, Investigation.

Declaration of competing interest

The authors declare that they have no known competing financial interests or personal relationships that could have appeared to influence the work reported in this paper.

Acknowledgments

This study was financially supported by grants from the Natural Science Foundation of China (82071104), Science and Technology Commission of Shanghai Municipality (23XD1434200/22Y21901000), Shanghai Hospital Development Center (SHDC12022120), National Clinical Research Center for Oral Diseases (NCRCO2021-omics-07), Shanghai Clinical Research Center for Oral Diseases (19MC1910600), Major and Key Cultivation Projects of Ninth People's Hospital affiliated to Shanghai Jiao Tong university School of Medicine(JYZP006), Shanghai's Top Priority Research Center (2022ZZ01017), CAMS Innovation Fund for Medical Sciences (2019-I2M-5-037), Fundamental research program funding of Ninth People's Hospital affiliated to Shanghai Jiao Tong University School of Medicine(JYZZ237), Eastern Talent Plan Leading Project (BJZH2024001), and partly supported by the Shanghai Ninth People's Hospital affiliated with Shanghai Jiao Tong University, School of Medicine (JYJC202223).

The authors would like to thank Shanghai Key Laboratory of Translational Medicine on Ear and Nose diseases (14DZ2260300) for experimental guidance of using the confocal laser scanning microscope.

Appendix A. Supplementary data

Supplementary data to this article can be found online at <https://doi.org/10.1016/j.mtbio.2025.101499>.

Data availability

Data will be made available on request.

References

- [1] F. Eggmann, J.M. Ayub, J. Conejo, M.B. Blatz, Deep margin elevation-Present status and future directions, *J. Esthetic Restor. Dent.* 35 (1) (2023) 26–47.
- [2] R.A. Bresser, D. Gerdolle, I.A. van den Heijkant, L.M.A. Sluiter-Pouwels, M.S. Cune, M.M.M. Gresnigt, Up to 12 years clinical evaluation of 197 partial indirect restorations with deep margin elevation in the posterior region, *J. Dent.* 91 (2019) 103227.
- [3] A.A. Balhaddad, I.M. Garcia, L. Mokeem, M.S. Ibrahim, F.M. Collares, M.D. Weir, H.H.K. Xu, M.A.S. Melo, Bifunctional composites for biofilms modulation on cervical restorations, *J. Dent. Res.* 100 (10) (2021) 1063–1071.
- [4] J. Juloski, S. Köken, M. Ferrari, Cervical margin relocation in indirect adhesive restorations: a literature review, *J. Prosthodont Res* 62 (3) (2018) 273–280.
- [5] H. Ghaemina, M.E. Nienhuijs, V. Toedtling, J. Perry, M. Tummers, T. J. Hoppenreijns, W.J. Van der Sanden, T.G. Mettes, Surgical removal versus retention for the management of asymptomatic disease-free impacted wisdom teeth, *Cochrane Database Syst. Rev.* 5 (5) (2020) CD003879.
- [6] L. Moreira-Souza, L. Butini Oliveira, H. Gaëta-Araujo, M. Almeida-Marques, L. Asprino, A.C. Oenning, Comparison of CBCT and panoramic radiography for the assessment of bone loss and root resorption on the second molar associated with third molar impaction: a systematic review, *Dentomaxillofacial Radiol.* 51 (3) (2022) 20210217.
- [7] M. Ferrari, S. Köken, S. Grandini, E. Ferrari Cagidiaco, T. Joda, N. Discepoli, Influence of cervical margin relocation (CMR) on periodontal health: 12-month results of a controlled trial, *J. Dent.* 69 (2018) 70–76.

- [8] G. Huang, M. Yang, M. Qali, T.J. Wang, C. Li, Y.C. Chang, Clinical considerations in orthodontically forced eruption for restorative purposes, *J. Clin. Med.* 10 (24) (2021) 5950.
- [9] M. Marzadori, M. Stefanini, M. Sangiorgi, I. Mounssif, C. Monaco, G. Zucchelli, Crown lengthening and restorative procedures in the esthetic zone, *Periodontol.* 2000 77 (1) (2018) 84–92.
- [10] G. Spagnuolo, Bioactive dental materials: the current status, *Materials* 15 (6) (2022) 2016.
- [11] S. Imazato, T. Kohno, R. Tsuboi, P. Thongthai, H.H. Xu, H. Kitagawa, Cutting-edge filler technologies to release bio-active components for restorative and preventive dentistry, *Dent. Mater. J.* 39 (1) (2020) 69–79.
- [12] G. Schmalz, R. Hickel, R.B. Price, J.A. Platt, Bioactivity of dental restorative materials: FDI policy statement, *Int. Dent. J.* 73 (1) (2023) 21–27.
- [13] S. Imazato, S. Ma, J.H. Chen, H.H. Xu, Therapeutic polymers for dental adhesives: loading resins with bio-active components, *Dent. Mater.* 30 (1) (2014) 97–104.
- [14] L. Han, T. Okiji, Evaluation of the ions release/incorporation of the prototype S-PRG filler-containing endodontic sealer, *Dent. Mater. J.* 30 (6) (2011) 898–903.
- [15] K. Ikemura, F.R. Tay, Y. Kouro, T. Endo, M. Yoshiyama, K. Miyai, D.H. Pashley, Optimizing filler content in an adhesive system containing pre-reacted glass-ionomer fillers, *Dent. Mater.* 19 (2) (2003) 137–146.
- [16] S. Imazato, T. Nakatsuka, H. Kitagawa, J.I. Sasaki, S. Yamaguchi, S. Ito, H. Takeuchi, R. Nomura, K. Nakano, Multiple-ion releasing bioactive surface pre-reacted glass-ionomer (S-PRG) filler: innovative Technology for dental treatment and Care, *J. Funct. Biomater.* 14 (4) (2023) 236.
- [17] H. Miyaji, K. Mayumi, S. Miyata, E. Nishida, K. Shitomi, A. Hamamoto, S. Tanaka, T. Akasaka, Comparative biological assessments of endodontic root canal sealer containing surface pre-reacted glass-ionomer (S-PRG) filler or silica filler, *Dent. Mater. J.* 39 (2) (2020) 287–294.
- [18] K. Yamaguchi-Ueda, Y. Akazawa, K. Kawarabayashi, A. Sugimoto, H. Nakagawa, A. Miyazaki, R. Kurogoushi, K. Iwata, T. Kitamura, A. Yamada, T. Hasegawa, S. Fukumoto, T. Iwamoto, Combination of ions promotes cell migration via extracellular signal-regulated kinase 1/2 signaling pathway in human gingival fibroblasts, *Mol. Med. Rep.* 19 (6) (2019) 5039–5045.
- [19] Y. Fujimoto, M. Iwasa, R. Murayama, M. Miyazaki, A. Nagafuji, T. Nakatsuka, Detection of ions released from S-PRG fillers and their modulation effect, *Dent. Mater. J.* 29 (4) (2010) 392–397.
- [20] H. Kitagawa, S. Miki-Oka, G. Mayanagi, Y. Abiko, N. Takahashi, S. Imazato, Inhibitory effect of resin composite containing S-PRG filler on *Streptococcus mutans* glucose metabolism, *J. Dent.* 70 (2018) 92–96.
- [21] S. Miki, H. Kitagawa, R. Kitagawa, W. Kiba, M. Hayashi, S. Imazato, Antibacterial activity of resin composites containing surface pre-reacted glass-ionomer (S-PRG) filler, *Dent. Mater.* 32 (9) (2016) 1095–1102.
- [22] M. Iijima, S. Ito, S. Nakagaki, N. Kohda, T. Muguruma, T. Saito, I. Mizoguchi, Effects of immersion in solution of an experimental toothpaste containing S-PRG filler on like-remineralizing ability of etched enamel, *Dent. Mater. J.* 33 (3) (2014) 430–436.
- [23] S.H. Bassir, W. Wisitrasameewong, J. Raanan, S. Ghaffarigarakani, J. Chung, M. Freire, L.C. Andrada, G. Intini, Potential for stem cell-based periodontal therapy, *J. Cell. Physiol.* 231 (1) (2016) 50–61.
- [24] P.M. Bartold, S. Gronthos, Standardization of criteria defining periodontal ligament stem cells, *J. Dent. Res.* 96 (5) (2017) 487–490.
- [25] Y. Sun, Z. Zhao, Q. Qiao, S. Li, W. Yu, X. Guan, A. Schneider, M.D. Weir, H.H.K. Xu, K. Zhang, Y. Bai, Injectable periodontal ligament stem cell-metformin-calcium phosphate scaffold for bone regeneration and vascularization in rats, *Dent. Mater.* 39 (10) (2023) 872–885.
- [26] X.Y. Xu, X. Li, J. Wang, X.T. He, H.H. Sun, F.M. Chen, Concise review: periodontal tissue regeneration using stem cells: strategies and translational considerations, *Stem Cells Transl Med* 8 (4) (2019) 392–403.
- [27] N. Ilie, T.J. Hilton, S.D. Heintze, R. Hickel, D.C. Watts, N. Silikas, J.W. Stansbury, M. Cadenaro, J.L. Ferracane, Academy of Dental Materials guidance-Resin composites: Part I-Mechanical properties, *Dent. Mater.* 33 (8) (2017) 880–894.
- [28] M. Par, Z. Tarle, R. Hickel, N. Ilie, Mechanical properties of experimental composites containing bioactive glass after artificial aging in water and ethanol, *Clin. Oral Invest.* 23 (6) (2019) 2733–2741.
- [29] M.A. Ashraf, W. Peng, Y. Zare, K.Y. Rhee, Effects of size and aggregation/agglomeration of nanoparticles on the interfacial/interphase properties and tensile strength of polymer nanocomposites, *Nanoscale Res. Lett.* 13 (1) (2018) 214.
- [30] P. Jitaluk, K. Ratanakupt, K. Kiatsirirote, Effect of surface prereacted glass ionomer nanofillers on fluoride release, flexural strength, and surface characteristics of polymethylmethacrylate resin, *J. Esthetic Restor. Dent.* 34 (8) (2022) 1272–1281.
- [31] R.G. Craig, F.A. Peyton, Elastic and mechanical properties of human dentin, *J. Dent. Res.* 37 (4) (1958) 710–718.
- [32] A. Alrahlah, A.B. Al-Odayni, W.S. Saeed, A. Al-Kahtani, F.M. Alkhtani, N.S. Al-Maflehi, Water sorption, water solubility, and rheological properties of resin-based dental composites incorporating immobilizable eugenol-derivative monomer, *Polymers* 14 (3) (2022) 366.
- [33] S. Gao, R. Liu, H. Xin, H. Liang, Y. Wang, J. Jia, The surface characteristics, microstructure and mechanical properties of PEEK printed by fused deposition modeling with different raster angles, *Polymers* 14 (1) (2021) 77.
- [34] M. Par, A. Gubler, T. Attin, Z. Tarle, A. Tarle, T.T. Tauböck, Ion release and hydroxyapatite precipitation of resin composites functionalized with two types of bioactive glass, *J. Dent.* 118 (2022) 103950.
- [35] N. Taghvaei, M. Ghavami-Lahiji, M. Evazalipour, R. Tayefeh Davaloo, E. Zamani, Ion release, biocompatibility, and bioactivity of resin-modified calcium hydroxide cavity liners, *BMC Oral Health* 23 (1) (2023) 1034.
- [36] Z. Ciosek, K. Kot, D. Kosik-Bogacka, N. Lanocha-Arendarczyk, I. Rotter, The effects of calcium, magnesium, phosphorus, fluoride, and lead on bone tissue, *Biomolecules* 11 (4) (2021) 506.
- [37] M.R. Shahrouzifar, E. Salahinejad, E. Sharifi, Co-incorporation of strontium and fluorine into diopside scaffolds: bioactivity, biodegradation and cytocompatibility evaluations, *Mater. Sci. Eng., C* 103 (2019) 109752.
- [38] N. Hirayama, T. Karaki, M. Onaga, R. Usuba, Y. Idaira, Y. Asada, Comparisons of retention rate and caries preventive effect between sealant containing S-PRG filler and resin-based sealant in children, *Jpn. J. Pediatr. Dent.* 57 (2019) 54–65.
- [39] N. Kaga, F. Nagano-Takebe, T. Nezu, T. Matsuura, K. Endo, M. Kaga, Protective effects of GIC and S-PRG filler restoratives on demineralization of bovine enamel in lactic acid solution, *Materials* 13 (9) (2020) 2140.
- [40] L. Tammaro, V. Vittoria, A. Calarco, O. Petillo, F. Riccitello, G. Peluso, Effect of layered double hydroxide intercalated with fluoride ions on the physical, biological and release properties of a dental composite resin, *J. Dent.* 42 (1) (2014) 60–67.
- [41] K. Nishida, T. Anada, S. Kobayashi, T. Ueda, M. Tanaka, Effect of bound water content on cell adhesion strength to water-insoluble polymers, *Acta Biomater.* 134 (2021) 313–324.
- [42] A.N. Gargalionis, C. Adamopoulos, C.T. Vottis, A.G. Papavassiliou, E.K. Basdra, Runx2 and polycystins in bone mechanotransduction: challenges for therapeutic opportunities, *Int. J. Mol. Sci.* 25 (10) (2024) 5291.
- [43] S. Maurotti, R. Mare, R. Pujia, Y. Ferro, E. Mazza, S. Romeo, A. Pujia, T. Montalcini, Hemp seeds in post-arthroplasty rehabilitation: a pilot clinical study and an in vitro investigation, *Nutrients* 13 (12) (2021) 4330.
- [44] H. Ma, H. Han, X. Zhao, J. Ma, X. Qu, X. Lou, A. Suonan, B. Lei, Y. Zhang, Engineering multifunctional polyether ether ketone implant: mechanics-adaptability, biomineralization, immunoregulation, anti-infection, osteointegration, and osteogenesis, *Adv. Healthcare Mater.* 12 (12) (2023) e2202799.
- [45] S. Vimalraj, Alkaline phosphatase: structure, expression and its function in bone mineralization, *Gene* 754 (2020) 144855.
- [46] A.F. Siller, M.P. Whyte, Hypophosphatasia and the role of alkaline phosphatase in skeletal mineralization, *Endocr. Rev.* 15 (4) (1994) 439–461.
- [47] Q. Wang, P. Li, P. Tang, X. Ge, F. Ren, C. Zhao, J. Fang, K. Wang, L. Fang, Y. Li, C. Bao, X. Lu, K. Duan, Experimental and simulation studies of strontium/fluoride-codoped hydroxyapatite nanoparticles with osteogenic and antibacterial activities, *Colloids Surf. B Biointerfaces* 182 (2019) 110359.
- [48] Z. Wu, Q. Tian, J. Wang, Y. Feng, L. Li, C. Xu, J. Lv, Z. Lv, A bone implant with NIR-responsiveness for eliminating osteosarcoma cells and promoting osteogenic differentiation of BMSCs, *Colloids Surf. B Biointerfaces* 211 (2022) 112296.
- [49] F. Perret, M. Aimetti, M. Andreasi Bassi, Hard and soft tissue augmentation with occlusive titanium barriers in jaw vertical defects: a novel approach, *Plast Aesthet Res* 9 (2022) 7.
- [50] A. Nemoto, N. Chosa, S. Kyakumoto, S. Yokota, M. Kamo, M. Noda, A. Ishisaki, Water-soluble factors eluted from surface pre-reacted glass-ionomer filler promote osteoblastic differentiation of human mesenchymal stem cells, *Mol. Med. Rep.* 17 (3) (2018) 3448–3454.
- [51] L. Qiao, X. Liu, Y. He, J. Zhang, H. Huang, W. Bian, M.M. Chilufya, Y. Zhao, J. Han, Progress of signaling pathways, stress pathways and epigenetics in the pathogenesis of skeletal fluorosis, *Int. J. Mol. Sci.* 22 (21) (2021) 11932.
- [52] A.V. Skalny, M. Aschner, E.V. Silina, V.A. Stupin, O.N. Zaitsev, T.I. Sotnikova, S. I. Tazina, F. Zhang, X. Guo, A.A. Tinkov, The role of trace elements and minerals in osteoporosis: a review of epidemiological and laboratory findings, *Biomolecules* 13 (6) (2023) 1006.
- [53] Z. Geng, L. Ji, Z. Li, J. Wang, H. He, Z. Cui, X. Yang, C. Liu, Nano-needle strontium-substituted apatite coating enhances osteoporotic osseointegration through promoting osteogenesis and inhibiting osteoclastogenesis, *Bioact. Mater.* 6 (4) (2020) 905–915.
- [54] D. Cheng, R. Ding, X. Jin, Y. Lu, W. Bao, Y. Zhao, S. Chen, C. Shen, Q. Yang, Y. Wang, Strontium ion-functionalized nano-hydroxyapatite/chitosan composite microspheres promote osteogenesis and angiogenesis for bone regeneration, *ACS Appl. Mater. Interfaces* 15 (16) (2023) 19951–19965.
- [55] F. Yang, D. Yang, J. Tu, Q. Zheng, L. Cai, L. Wang, Strontium enhances osteogenic differentiation of mesenchymal stem cells and in vivo bone formation by activating wnt/catenin signaling, *Stem Cells (Dayton, Ohio)* 29 (2011) 981–991.
- [56] Z. Gong, H. Cheng, M. Zhang, X. Liu, Y. Zeng, K. Xiang, Y. Xu, Y. Wang, Z. Zhu, Osteogenic activity and angiogenesis of a SrTiO₃ nano-gridding structure on titanium surface, *J. Mater. Chem. B* 5 (3) (2017) 537–552.
- [57] Z. Wu, J. Bai, G. Ge, T. Wang, S. Feng, Q. Ma, X. Liang, W. Li, W. Zhang, Y. Xu, K. Guo, W. Cui, G. Zha, D. Geng, Regulating macrophage polarization in high glucose microenvironment using lithium-modified bioglass-hydrogel for diabetic bone regeneration, *Adv. Healthcare Mater.* 11 (1) (2022) e2200298.
- [58] S. Wiszniak, Q. Schwarz, Exploring the intracrine functions of VEGF-A, *Biomolecules* 11 (1) (2021) 128.